Surface and bulk characterization of an ultrafine South African coal fly ash with reference to polymer applications

E. M. van der Merwe[a*], L.C. Prinsloo[b], C. L. Mathebula[a], H.C. Swart[c], E. Coetsee[c] and F.J. Doucet[d]

[a] *Department of Chemistry, University of Pretoria, Lynnwood Rd, Pretoria, 0002 South Africa*

[b] *Department of Physics, University of Pretoria, Lynnwood Rd, Pretoria, 0002 South Africa*

[c] *Department of Physics, University of the Free State, P.O. Box 339, Bloemfontein 9300, South Africa*

[d] *Mineral Waste Beneficiation Group, Council for Geoscience, 280 Pretoria Rd, Private Bag X112, Pretoria 0001, South Africa*

***Corresponding author:** liezel.vandermerwe@up.ac.za; +27 12 420 5379

Abstract

South African coal-fired power stations produce about 25 million tons of fly ash per annum, of which only approximately 5% is currently reused. A growing concern about pollution and increasing landfill costs stimulates research into new ways to utilize coal fly ash for economically beneficial applications. Fly ash particles may be used as inorganic filler in polymers, an application which generally requires the modification of their surface properties. In order to design experiments that will result in controlled changes in surface chemistry and morphology, a detailed knowledge of the bulk chemical and mineralogical compositions of untreated fly ash particles, as well as their morphology and surface properties, is needed. In this paper, a combination of complementary bulk and surface techniques was explored to assess the physicochemical properties of a classified, ultrafine coal fly ash sample, and the findings were discussed in the context of polymer application as fillers. The sample was categorized as a class F fly ash (XRF). 62% of the sample was an amorphous glass phase, with mullite and quartz being the main identified crystalline phases (XRD, FTIR). Quantitative carbon and sulphur analysis reported a total bulk carbon and sulphur content of 0.37% and 0.16% respectively. The spatial distribution of the phases was determined by 2D

mapping of Raman spectra, while TGA showed a very low weight loss for temperatures ranging between 25 and 1000°C. Individual fly ash particles were characterised by a monomodal size distribution (PSD) of spherical particles with smooth surfaces (SEM, TEM, AFM), and a mean particle size of 4.6 µm (PSD). The BET active surface area of this sample was 1.52 m^2/g and the chemical composition of the fly ash surface (AES, XPS) was significantly different from the bulk composition and varied considerably between spheres. Many properties of the sample (*e.g.* spherical morphology, small particle size, thermal stability) appeared to be suitable for its applicability as filler in polymers, although the wide variation in surface composition between individual particles may challenge the development of a suitable surface modification technique. The observation that the bulk and surface compositions of the particles were so intrinsically different, strongly suggested that surface characterization is important when considering compatibility between matrices when applying fly ash as filler in polymers.

Keywords: Coal fly ash, bulk properties, surface properties, characterization

1. Introduction

Coal fly ash (FA) is one of the main residues produced during the combustion of pulverized coal in thermoelectric power stations. It originates from the lighter particles ascending with the flue gases during coal combustion, and is collected by electrostatic precipitators or bag filter systems. After precipitation, collected FA is safely disposed of and managed on ash dumps or slurry dams; or it can be utilized in a number of applications. FA is usually classified by particle size, creating a relatively uniform fine grey powder of which the particles are predominantly spherical in shape. Depending on the source and type of coal being combusted, the FA composition may differ considerably, but its chemical nature remains predominantly glassy or amorphous **[1]**.

The main source of power generation in South Africa is coal-fired thermoelectric power stations, which currently produce about 25 million tons of FA per annum **[2]**. Approximately 5% of the produced FA is reused, mainly as cement extender and in the production of concrete. In addition,

SASOL Synfuels generates an additional 4 million tons of fine ash per annum **[3]**. The extensive amounts of FA that is produced each year pose significant environmental and economic threats due to the great need of environmentally safe and economically affordable ways of disposal and handling. There is a growing concern about pollution and increasing landfill costs and therefore there has been global interest in the utilization of FA for economically beneficial applications.

South Africa has a long history regarding the development of new applications for FA. The beneficiation of South African FA after it has been put through a process of air classification, electrostatic recovery and/or density separation has been described before **[1]**, and specific size fractions of FA, with specific physical and chemical properties, may be used in suitable applications. The country's research and development involving FA includes its application in building and construction as cement extender and into lightweight aggregates [4], environmental rehabilitation in the form of counteracting acid mine drainage, wastewater treatment, and toxic element immobilization by zeolites [5-7], mine backfilling, the recovery of alumina [8, 9], production of geopolymers [10, 11] and hydrotalcites [12], soil amelioration [13], refractories and bricks, road stabilization, CO_2 capture [14], and as a processing aid and functional filler in polymers [15].

In order to take advantage of FA utilization efficiently, an accurate characterization of the chemical composition and mineralogy of a FA sample from a specific origin needs to be performed [16]. Furthermore, if the targeted applications require surface modification of FA, the properties of its surface need to be characterised appropriately.

Very few studies have specifically described the characterisation of South African FA samples [2, 17, 18], and due to differences in origin and method of classification and/or separation, the physical and chemical properties of FA products will vary. Furthermore, the industrial application of FA will dictate which physical and chemical properties need to be characterised.

In order to understand the processes that can enhance the properties of FA for its industrial application into polymers, a detailed study of the surface, chemical and morphological properties of FA is necessary before experimentation according to scientific methods can take place. Apart from controlling the mechanical properties (e.g. toughness, stiffness, and strength) of polymer composites, the viscosity of the uncured mixture must be low enough to improve workability and permit the evacuation of air bubbles. Studies performed by Roulin-Moloney [19] and Nakamura [20] have shown that increasing the particle size of spherical silica particles in a silica-filled epoxy resin have a detrimental effect on the strength of the obtained composite. The mean particle size range studied by Roulin-Moloney was between 60 - 300 µm, while that of Nakamura ranged between 6 – 42 µm. On the other hand, the same authors have noted that although the use of filler particles with sizes less than 4.5 µm may improve the strength of the composite, a practical limit is enforced by the viscosity of the mixture. Smaller filler particles have a greater surface area and may thus considerably increase the viscosity of the uncured filler-polymer mixture. It is therefore clear that particle size will have a considerable effect on the properties of polymer-filler composites, and this effect will be material-specific. Due to the increased mechanical properties obtained upon decrease in filler particle size, an ultrafine coal fly ash sample was chosen for the purpose of this study.

In this paper, a comprehensive combination of complementary characterisation techniques was used to determine the chemical composition, mineralogy and surface properties of a classified South African FA sample. These results serve as a strong foundation in our ongoing project where we are designing and testing dry and wet coating procedures aimed at modifying the surface properties of FA particles according to specific requirements imposed by our targeted applications.

2. Materials and Methods

2.1 Origin and description of the ultrafine fly ash sample

A representative sample of a classified, ultrafine FA sample was obtained from the Ash Resources Pty Ltd's ash beneficiation site at Eskom's Lethabo Thermal Power station, which is located between Vereeniging and Sasolburg in the Free State province of South Africa. This commercial-grade FA is classified on site using electrostatic precipitators and is specified to have a mean particle size between 3.9 and 5.0 µm, with more than 90% **of the volume distribution** of its particles having a diameter smaller than 11 µm. After classification it is marketed as a very fine, spherical, pozzolanic and highly reactive alumino-silicate with a low carbon content. The product currently finds application in the construction industry, but is also used in small quantities in the rubber and polymer industries.

2.2 Bulk characterisation of the fly ash sample

2.2.1 X-ray fluorescence spectroscopy (XRF) analysis

XRF was used to determine the bulk chemical concentrations of major elements in the FA sample. No milling was required prior to the analyses. The analyses were performed on an ARL9400XP+ XRF spectrometer (Thermo ARL, Switzerland). The loss on ignition (LOI) was determined by roasting the sample at 1000 °C for at least 3 hours until a constant weight was obtained. A glass disk was prepared by fusing a mixture of 1 g of the fly ash sample with 6 g of $Li_2B_4O_7$ at 1000 °C.

2.2.2 X-ray diffraction (XRD) analysis

The mineralogical composition of the FA sample was obtained by XRD. The XRD patterns were collected from 5° to 90° on a PANalyticalX'Pert Pro powder diffractometer with X'Celerator detector and variable divergence and fixed receiving slits with Fe filtered Co-Kα radiation. The phases were identified using X'PertHighscore plus software. The relative phase amounts were estimated using the Rietveld method (Autoquan Program). Twenty percent silicon (Aldrich 99% pure) was also

added to each sample for the determination of amorphous content. The samples were then micronized in a McCrone micronizing mill, and prepared for XRD analysis using a back loading preparation method.

2.2.3 Carbon and Sulphur analysis

The total carbon and sulphur content of the FA sample was determined using an Eltra CS 800 Double Dual Range system. Between 50 and 200 mg of sample was weighed into a ceramic crucible. Iron and tungsten chips were added, mixed and then combusted in a stream of oxygen where carbon and sulphur was converted into CO_2 and SO_2 respectively. The concentrations of gasses were detected using four infrared absorption detectors. The instrument was calibrated using certified carbon and sulphur standards, Euronorm-CRM 484-1 Whiteheart malleable iron and Leco No 501-502. The reported result is the average of two measurements.

2.2.4 Thermogravimetric analysis (TGA)

TGA analyses were performed on a Mettler Toledo TGA/SDTA 851e Thermogravimetric Analyzer. Approximately 20 mg of sample was placed in an alumina pan and heated from 25 - 1000 °C at a heating rate of 10 ºC/min. Thereafter, the sample was kept isothermally at 1000 °C for 10 minutes. Air was used as the purge gas at a flow rate of 60 ml/min. Analysis of the sample was repeated five times, and the average weight loss for each step was determined.

2.2.5 Particle size distribution (PSD) analysis

The particle size distribution of the sample was obtained by laser diffraction using a Malvern Mastersizer 2000 (Malvern Instrument Ltd., Worcester, UK) fitted with a Hydro 2000G dispersion unit. Scattered light data were recorded from 2000 to 5000 snapshots of 10 µs. A polydisperse mode of analysis and a refractive index of 1.533 with an adsorption of 0.1 were chosen. Size data collection was performed at constant obscuration in the range 10–20%.

2.2.6 BET Surface area analysis

A Nova 1000e Surface Area and Pore Size Analyzer (Quantachrome Instruments, USA), using nitrogen gas as adsorbent, was used to determine the bulk surface area by the Brunauer, Emmet, and Teller theory. The sample was degassed at 350 °C for 3 hours before performing the gas adsorption tests. The measurement was performed in triplicate.

2.2.7 Scanning Electron Microscopy (SEM) imaging

To study the morphology of the fly ash, the powder was mounted on a double-sided carbon tape by dipping carbon stubs into the samples. Excess material was removed by gentle blowing with compressed nitrogen. The sample was then sputter-coated with carbon in a Emitech K550X (Ashford, England). A Zeiss Ultra SS (Germany) field emission scanning electron microscope (FESEM), operated at an acceleration voltage of 1 kV, was used under dry high-vacuum condition to observe the morphology of the FA particles and confirm their size distribution.

2.2.8 Transmission Electron Microscopy (TEM) imaging

A JEOL JEM 2100F TEM was used to study the topography of the FA particles. The samples were first dispersed in 100% ethanol with the aid of sonication. A drop of the diluted suspension was poured onto a copper grid which was then placed into the sample injection holder for analysis.

2.2.9 Atomic Force Microscopy (AFM) imaging

A Bruker Dimension Icon AFM was used to perform AFM imaging analysis. The cantilever tip used was a TESPA-Si doped tip, and a tapping mode was used at a tapping frequency of 0.6Hz. Each sample was prepared by placing the sample on a thin layer of Japan Gold varnish, spread onto a microscope slide.

2.2.10 Infrared spectroscopy (FTIR) analysis

Mid-infrared spectra were recorded with a Brüker 70v Fourier transform infrared (FTIR) spectrometer, by placing the finely grounded samples in a diamond ATR (attenuated total

reflection) cell. The resolution was 2 cm^{-1} and 32 scans were signal-averaged in each interferogram.

2.2.11 Raman spectroscopy mapping

The Raman mapping of the fly ash sample was recorded with a WiTec Alpha 300 RA equipped with a UHTS spectrometer and Newton CCD camera. A 20x Zeiss objective was used and the excitation source was a 532nm Nd. Yag laser. A 2D array of approximately 10 000 Raman spectra were recorded from the sample.

2.3 Surface characterisation of the fly ash sample

2.3.1 Auger electron spectroscopy (AES) analysis

AES measurements were performed using a PHI 700 Scanning Auger Nanoprobe. SEM images were obtained with a 25 kV and 10 nA electron beam. The base pressure of the system was $5x10^{-10}$ Torr. AES surveys were performed with a 25 kV 10 nA electron beam. The samples were cleaned with a 2 kV 2 µA 1x1 mm Ar ion gun with a sputter rate of 27 nm/min.

2.3.2 X-ray photoelectron spectroscospy (XPS) analysis

XPS measurements were performed at a take-off angle of 45° in a high resolution PHI 5000 Versaprobe ESCA (electron spectroscopy for chemical analysis) microprobe system. Survey scans were done using monochromatic Al Kα X-rays with a beam diameter of 100 µm. A pass energy of 11.75 eV was used for the detailed XPS scans. The accelerating voltage was 15 kV and the beam power 25 W. The possible chemical states were identified by using the Multipak computer software version 8.2c.

3. Results and Discussion

The physical performance of fly ash-polymer composites will depend on the characteristics of the filler, its dispersion properties and the strength of polymer-filler interactions. In order to understand these, the bulk physical and chemical properties of the filler need to be characterised. Furthermore, the properties of the interface and strength of the interaction between the fly ash filler and polymer need to be understood before any surface modification techniques are applied to the surface of the filler. For this reason, it is important to characterise the surface composition of the fly ash sample.

3.1 Bulk properties of the fly ash sample

3.1.1 Chemical and mineralogical characterisation

The fly ash sample was predominantly composed of an amorphous alumina silica glass phase (62.1%), and the two main crystalline phases were mullite (31.8%) and quartz (6.1%).

The elemental analysis of the fly ash sample was obtained by XRF (Table 1). The sample contains a very low percentage of moisture, sulphur, unburned carbon, carbonates and hydroxides as indicated by the low loss on ignition (LOI of 0.52%) value. An ASTM criterion (C618–80) [21] requires a maximum LOI value of 6% for fly ash to be used in Portland cement, while the European Standard (EN 206-1) [22] accepts a LOI of 5%. Most thermal power stations aim to minimise the fly ash LOI for a number of reasons, one being the loss of thermal energy for the power station. Furthermore, in order to reuse coal fly ash as partial replacement for Portland cement in concrete manufacture, the carbon content of the ash needs to be low to minimise its effect on air entrapment in the concrete product [23].

According to ASTM standard specification C618-93 [21], fly ash is classified according to its chemical composition, and the classification depends on the total amount of SiO_2 + Al_2O_3 + Fe_2O_3.

The total amount of these three phases in a Class F fly ash exceeds 70% while it is between 50 - 70% for a Class C fly ash. The amount of CaO in a Class F fly ash is lower than that of a Class C fly ash, and is typically less than 20%. The Class F classification of the studied fly ash sample was confirmed by XRF, as the percentage composition of CaO in the ash sample was found to be approximately 6%, while the total amount of SiO_2 + Al_2O_3 + Fe_2O_3 exceeded 90%.

The total alkaline content (Na_2O + K_2O) was less than 1%, while the total concentration of rare earth metals (CaO + MgO) was about 5%. The major constituents of this sample, reported as oxides, are SiO_2 (49.3%), Al_2O_3 (34.0%), Fe_2O_3 (5.8%), CaO (5.1%) and TiO_2 (2.0%). Similar results were obtained for fly ash samples from different locations within South Africa [6, 18].

The elemental analysis obtained from XRF is consistent with the different phases obtained from the XRD data, and the low amount of fluxing ions (Na^+, K^+, Ca^{2+},etc.) present indicates that the glass (amorphous phase) consists of a high percentage of silica and alumina.

3.1.2 Thermal stability

Industrially, the carbon content of coal fly ash serves as an indication of the efficiency of the coal combustion process during electricity generation. A higher carbon content indicates a higher loss of thermal energy during coal combustion, and is economically unviable. Recently, thermal analysis techniques have been applied widely in characterisation of the quantity and chemical form of the carbon contained in coal fly ash [24-27]. When coal fly ash is heated in air (oxidising environment), a weight loss in the temperature range 500-740 °C can be attributed to one or both of the following processes [27]:

$$2C(s) + xO_2(g) \rightarrow 2CO_x(g) \quad (x = 1 \text{ or } 2) \qquad (1)$$

$$CaCO_3(s) \rightarrow CaO(s) + CO_2(g) \qquad (2)$$

The results obtained from TGA analysis of this fly ash sample is presented in Figure 1. The initial weight gain is due to a buoyancy effect, as the density of the purge gas decreases with an

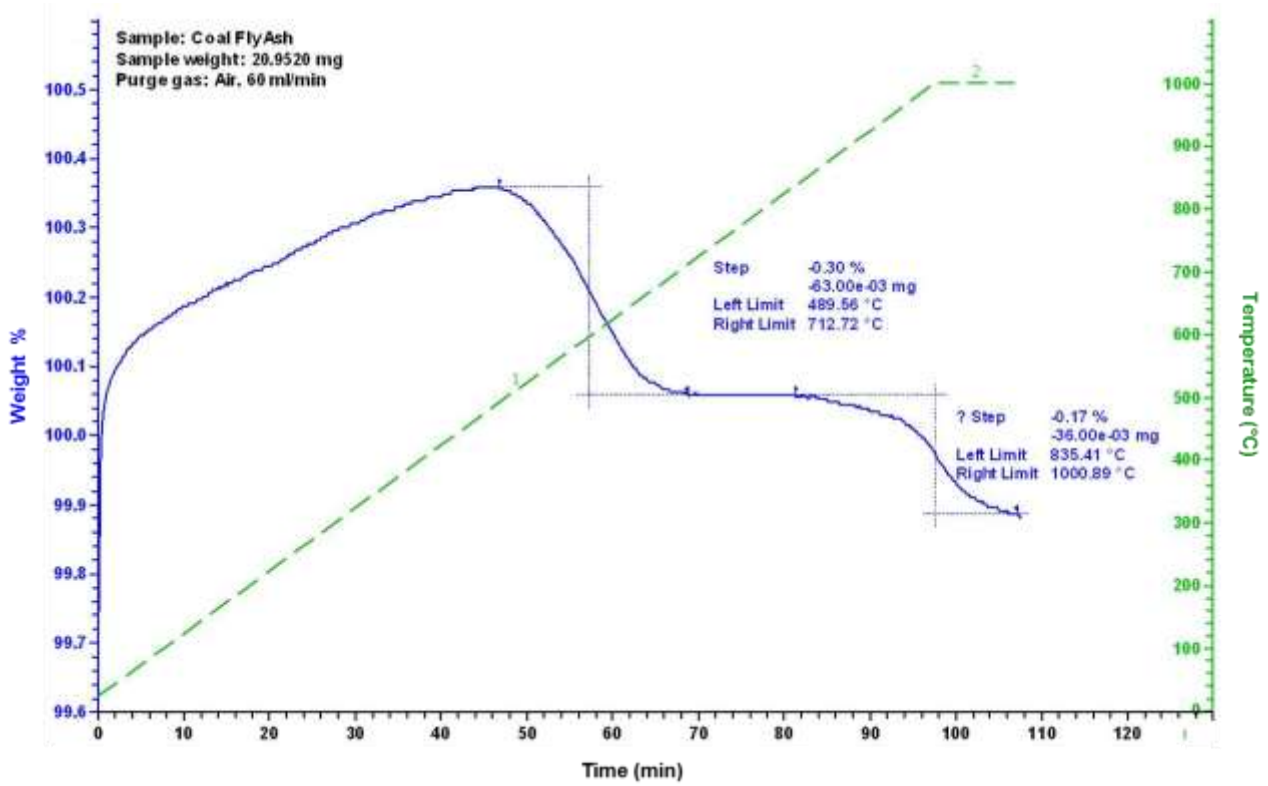

Figure 1: A representative thermogravimetric (TGA) curve of the fly ash sample

increase in temperature. Since the total weight loss observed for this sample is so low, the buoyancy effect seems more enhanced.

$CaCO_3$ was not detected in this sample by any of the analytical techniques used, which strongly suggested that the weight loss recorded between 489 – 712 °C can only be ascribed to the oxidation of carbon. The average (n = 5) weight loss obtained over this temperature range was 0.298 ± 0.014 %, indicating the amount of unburnt carbon present in this sample. This result corresponds well to the result obtained from Carbon and Sulphur analysis (0.37%).

The weight loss occurring from 835-1000°C can be attributed to the decomposition of anhydrite, $CaSO_4$ [28], which is described by the following reactions:

$$CaSO_4(s) \rightarrow CaO(s) + SO_3(g) \quad (3)$$

$$SO_3(g) \rightarrow SO_2(g) + \tfrac{1}{2}O_2(g) \quad (4)$$

Although no $CaSO_4$-containing phase was identified by XRD, the results obtained from XPS analysis confirmed the presence thereof (Table 3). This can possibly be attributed to a small amount of gypsum and/or anhydrite present in the FA sample. The decomposition temperature of pure anhydrite ($CaSO_4$) normally occurs at temperatures exceeding 1000°C under oxidising conditions, but Shimizu [29] reported a significant lowering in the decomposition temperature of $CaSO_4$ in the presence of coal fly ash. Results obtained from quantitative carbon and sulphur analysis indicated a sulphur content of 0.16%, which corresponds to a SO_3 content of 0.40%. The data obtained from XRF analyses presented a SO_3 content of 0.24%. The average weight loss of five TGA measurements is 0.169 ± 0.005 %, indicating the loss of SO_3 from the solid sample. This value is lower than the corresponding values obtained from the other two analytical techniques, and may serve as an indication that the decomposition of the sulphate contained in the sample during the TGA analysis is incomplete, or that other forms of sulphur (not detected by TGA) are present in the sample. Since the total amount of sulphur in this FA sample is so low, an adequate characterisation of the forms of sulphur present in the sample by TGA is not possible.

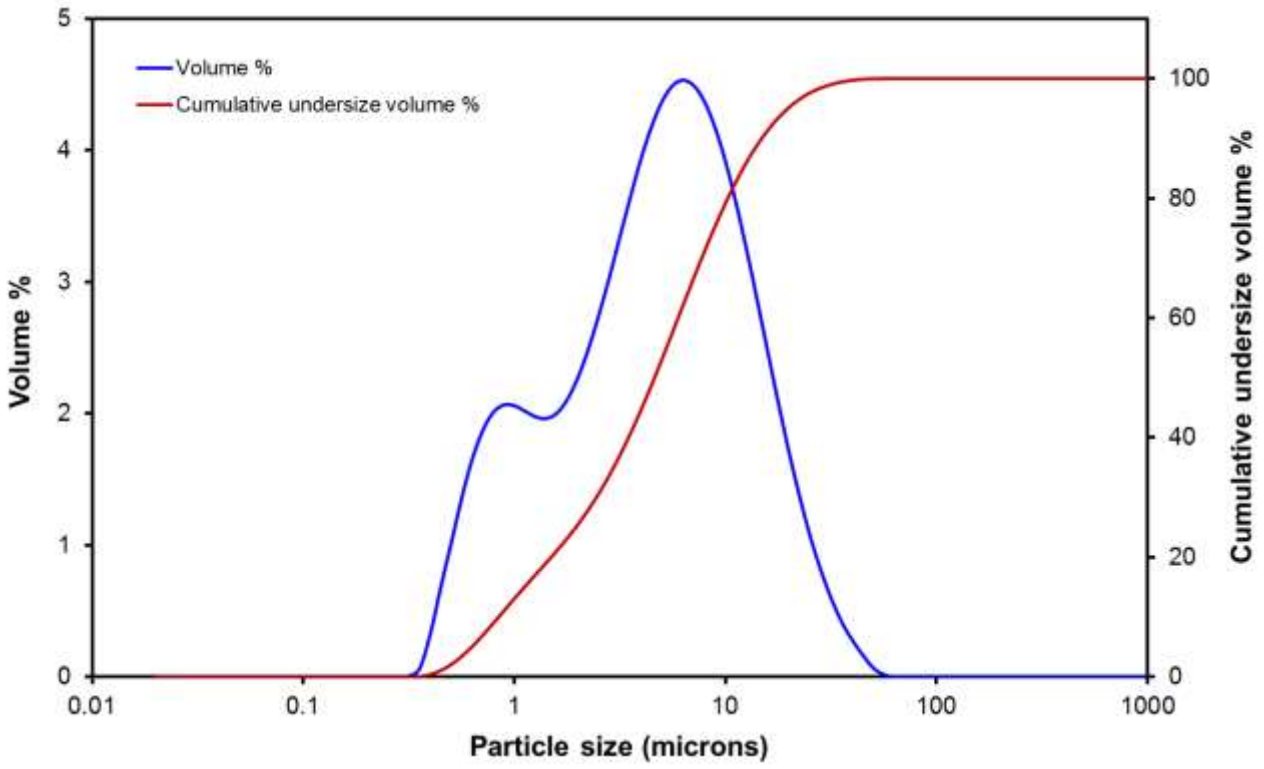

Figure 2: Particle size distribution of the FA sample

3.1.3 Particle size distribution and BET surface area

The lognormal particle size distribution of this sample was observed to be monomodal with a tail towards the lower particle sizes (Figure 2). The mean particle size is 4.6 µm, with 90% of the **volume distribution of the** sample having particle sizes smaller than 14.9 µm. This data corresponds well to the values specified by industry, mentioned earlier in this paper. The BET active surface area was determined to be very low (1.52 m^2/g).

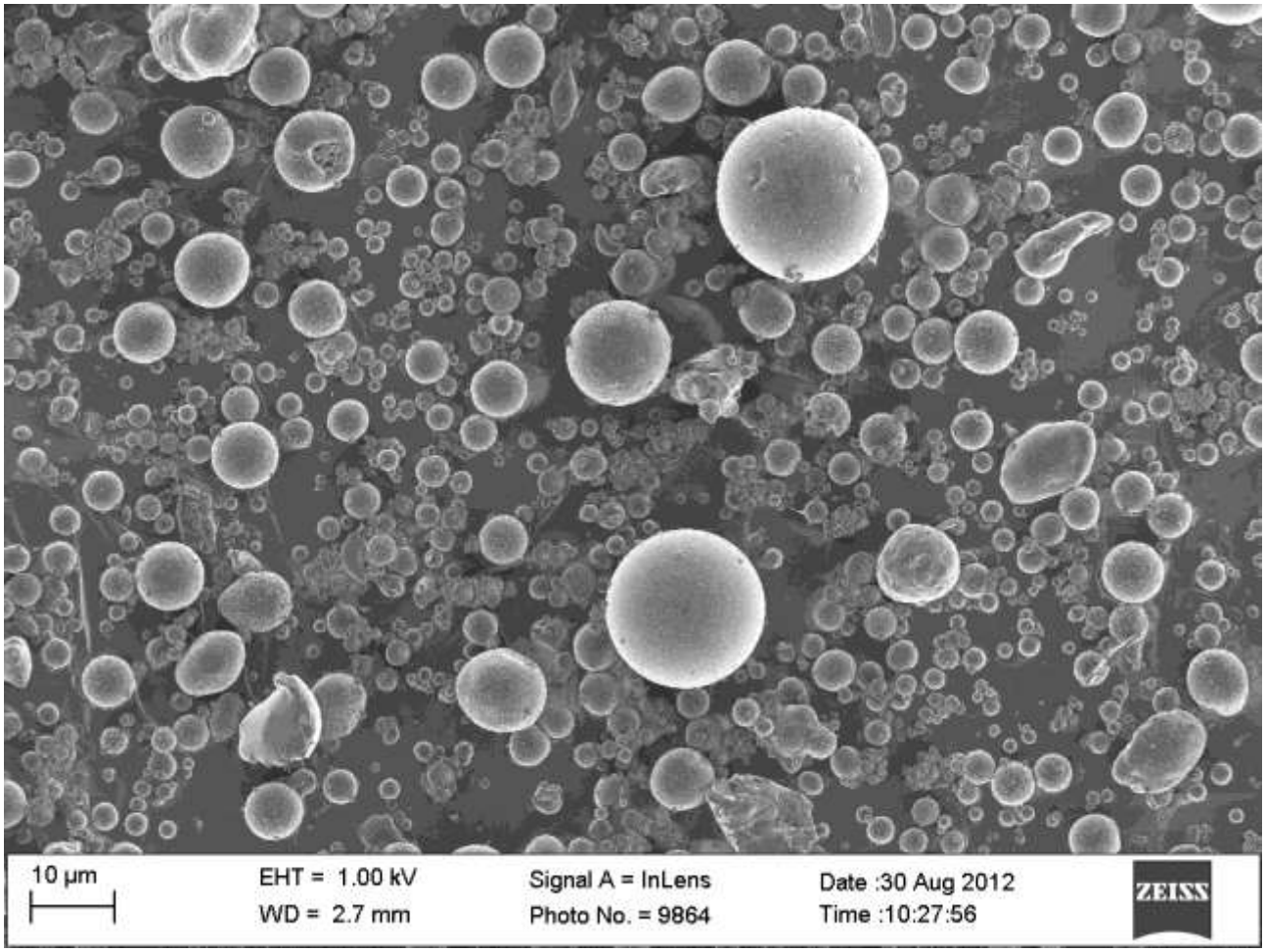

Figure 3: SEM micrograph of the coal fly ash sample, showing good sphericity and some agglomeration between the fly ash spheres

3.1.4 Morphological and topographic characterisation

The morphology of the sample as observed from SEM measurements is shown in Figure 3. The particle shape and distribution of the fly ash is reported to be spherical or “ball-bearing” with some

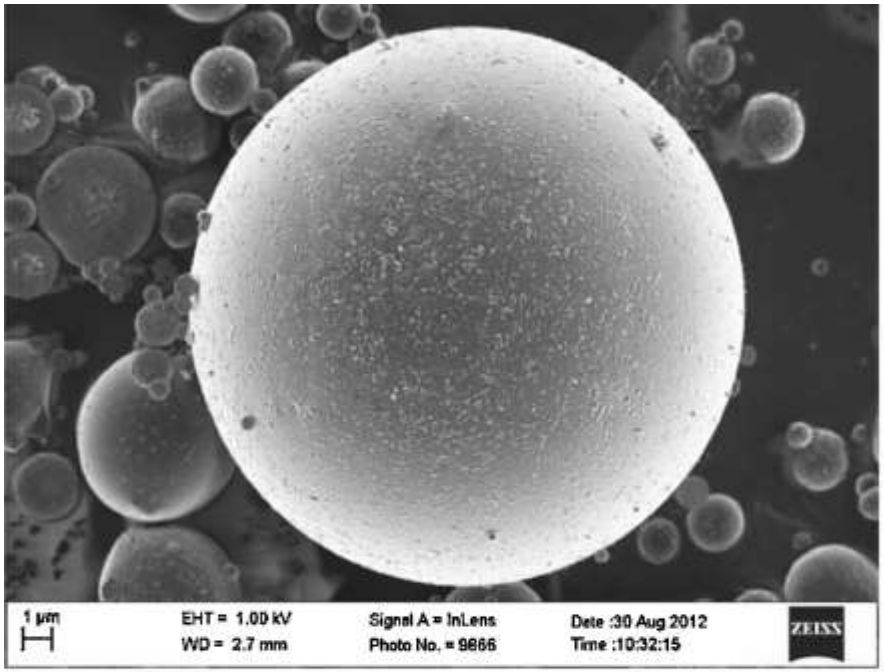

(a)

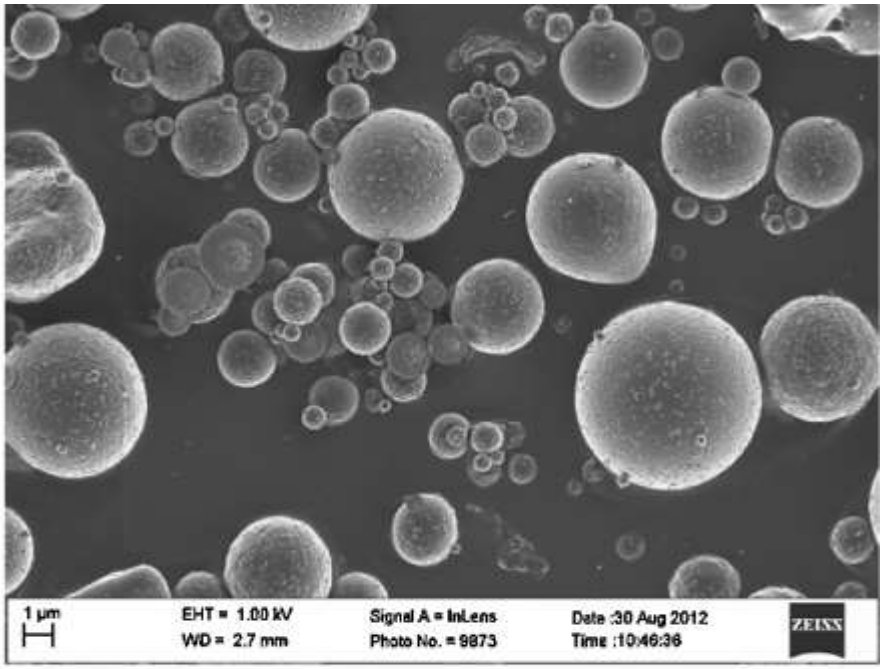

(b)

Figure 4(a) and (b): SEM micrographs of fly ash particles of different particle sizes (taken at similar magnification) showing the relatively smooth surface of the spheres

of the particles seen to be tightly attached to each other, forming agglomerates which might introduce problems with workability upon compaction of this type of fly ash into polymeric materials. These characteristics are clearly visible in the micrograph. Figure 4(a) shows a high-resolution SEM image of a larger fly ash sphere, taken at higher magnification, from which the relatively smooth surface of the spheres can be observed. Figure 4(b) was taken at the same magnification as Figure 4(a), and confirms that the surface topography of smaller spheres is similar to that of larger spheres (Figure 4(a)). The SEM results confirm the significant variation in particle size of the spheres, as observed by particle size determination.

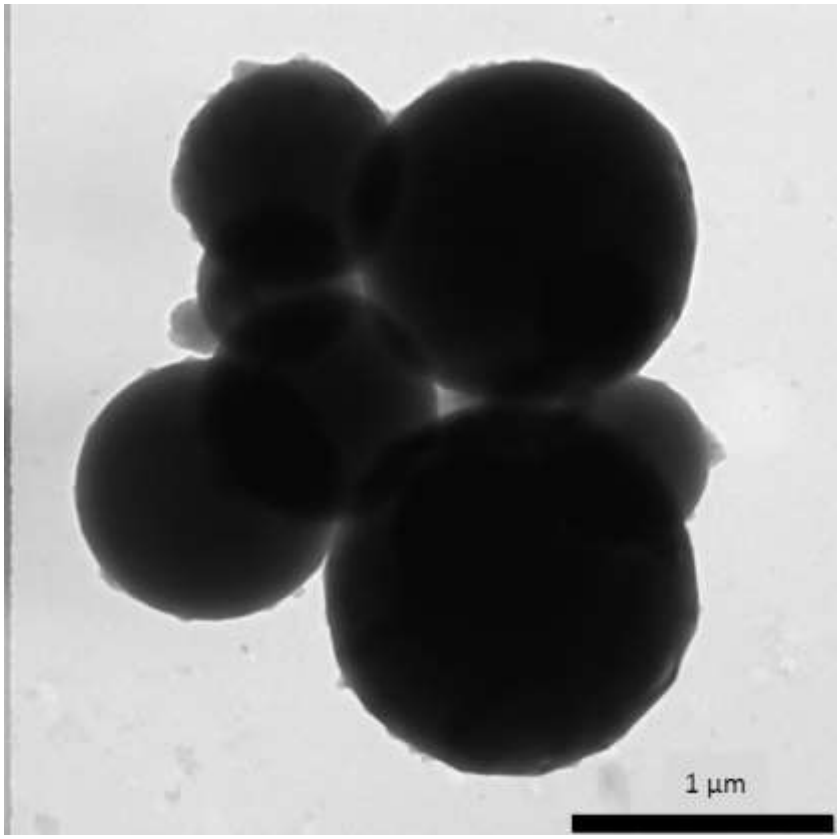

Figure 5: TEM micrograph of the studied coal fly ash sample

The spherical nature of the particles was confirmed by TEM (Figure 5). Most of the TEM images also show aggregates on the surface of the fly ash spheres, a result which is supported by SEM (Figure 4). The occurrence of these small aggregates on the surface of fly ash has been described by previous authors, and seems to be of carbonaceous nature. Both Chen [30] and Hower [31] have described the occurrence of carbonaceous aggregates on different types of fly ash particles.

Chen performed a TEM study on an ultrafine fly ash, and described the morphologies of the soot aggregates on the fly ash surface to have branching chain-like structures, with typical particle sizes ranging from 20 to 50 nm. The micro textures of these soot particles were described as consisting of concentrically stacked graphitic layers.

The results obtained by Chen [30] were confirmed by Hower [31], who demonstrated the presence of nanoscale carbonaceous particles on the surface of their fly ash sample by a combination of High-Resolution Transmission Electron Microscopy, Scanning Transmission Electron Microscopy, and Electron Energy-Loss Spectroscopy (HRTEM-STEM-EELS). These authors described the morphology of the particles on the fly ash surface as "C agglomerates with typical soot-like appearance and others with graphitic fullerene-like nanocarbon structures". Hower et al. further described these agglomerates to be associated with slightly larger aluminosilicate spheres, that they often form an ultrathin deposit on the fly ash surface, and that they may host very fine (<3 nm) metal and metal oxide particles.

Atomic Force Microscopy (AFM) is a generally used surface characterisation technique and its popularity is increasing because sample analysis can be performed at ambient conditions and sample preparation is minimal. The technique is well suited for individual particle analysis of powdered samples, and is able to provide a high-resolution topographical analysis of the surface of particles at the nano-scale. Direct measurements of particle height, particle volume and a 3D surface image can be obtained within a single measurement. The surface topography of coal fly ash by AFM has initially been described by Demanet [32], who reported that smaller fly ash spheres (diameters up to 10 μm) did not exhibit much structure on their surface. The results obtained from AFM imaging of a representative sphere of the fly ash used in this study is presented in Figure 6. The first image (Figure 6(a)) displays the three-dimensional representation of the surface of a glassy fly ash sphere. In order to minimise movement of the spheres during analysis, a varnish was used to set the fly ash sample, and therefore the obtained image is only the portion of the sphere emerging above the surface of the varnish. The height profile of the area

emerging above the varnish surface is shown in Figure 6(c), and corresponds to the cross-sectional lines presented on the two-dimensional image in Figure 6(b). These images confirm the smooth surface observed from SEM measurements of the same sample, and agrees well with the data recorded by Demanet [32]. In Figure 6(c), similar height profiles were obtained in all directions taken, indicating good sphericity of the glassy fly ash sphere studied.

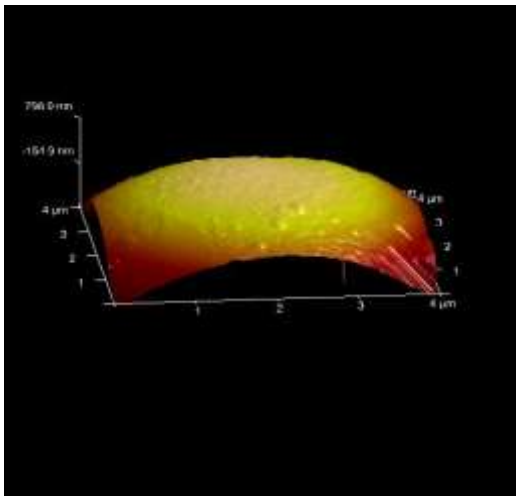

(a) 3D AFM image of a fly ash sphere, scan size 4 x 4 µm.

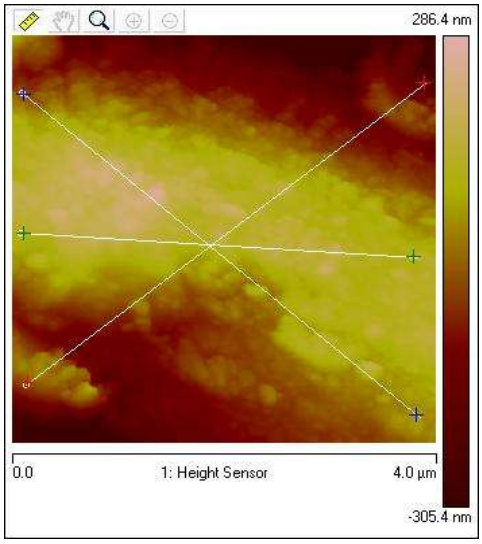

(b) 2D AFM image showing the cross-section lines, indicating positions where height profiles were obtained

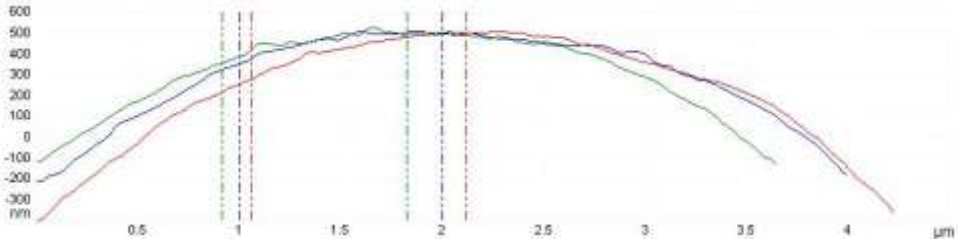

(c) 2D AFM Height profile of the surface of a fly ash sphere

Figure 6: AFM tapping mode images of a representative fly ash sphere; (a) 3D AFM image of a fly ash sphere, scan size 4 x 4 µm; (b) 2D AFM image showing the cross-section lines, indicating positions where height profiles were obtained, and c) 2D AFM Height profile of the surface of a fly ash sphere

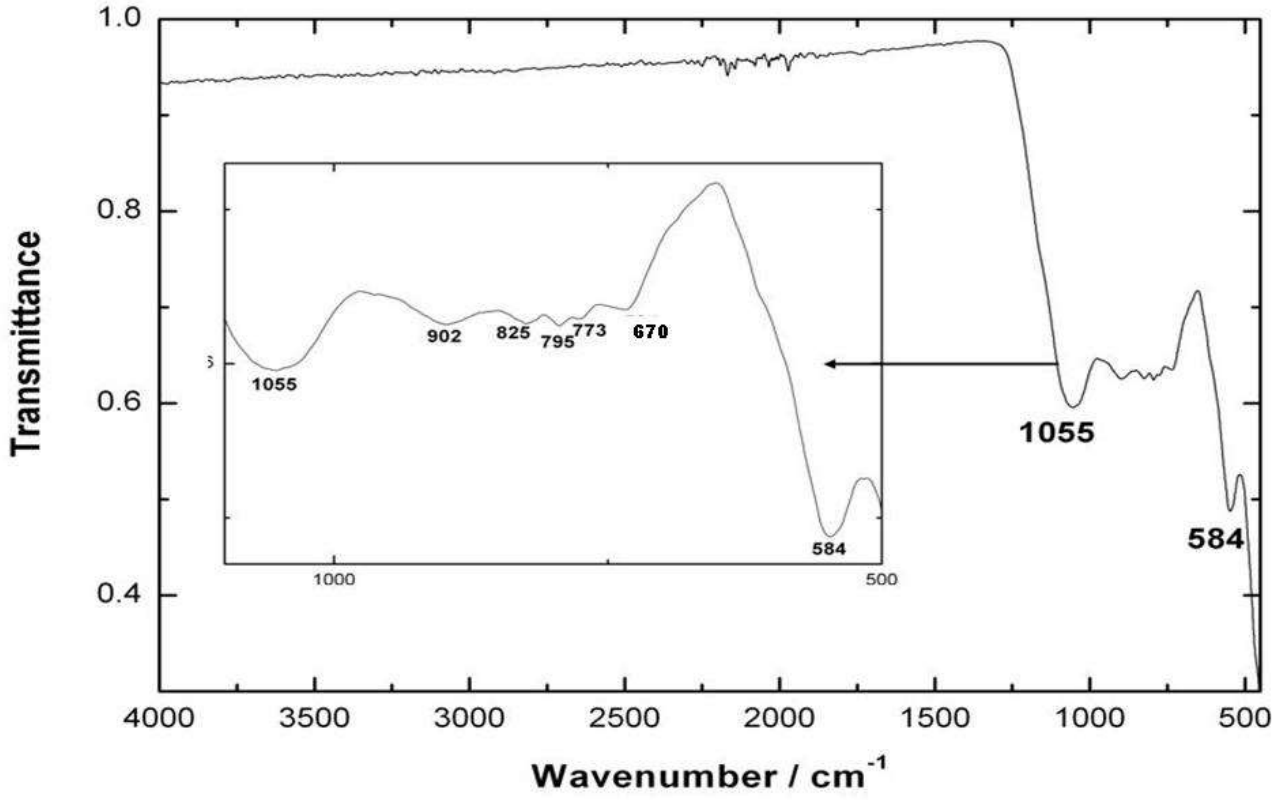

Figure 7: FTIR transmission spectrum of fly ash

3.1.5 Spectroscopic analysis

The mid-infrared transmission spectrum of the fly ash sample is presented in Figure 7 and is a superimposition of the FTIR spectra of silica glass, mullite and a small contribution of α-quartz (see fly ash composition, Table 1). The strongest peak in the FTIR spectrum was observed around 1000 cm^{-1} and was attributed to Si-O-Si asymmetric stretching vibrations and has contributions of glass, mullite and quartz. The band at 902 cm^{-1} originates from Al-O symmetric stretching vibrations from mullite [33, 34]. Al-O-Si symmetrical stretching vibrations occur at about 770 cm^{-1} [35, 36] and overlaps with the very characteristic doublet of quartz at 778 and 792 cm^{-1} (see insert Fig. 7). The peak at 670 cm^{-1} has contributions from quartz and mullite Al-O-Al bending vibrations [33, 34]. The 584 cm^{-1} peak belongs to Al-O stretching vibrations (mullite) and the 462 cm^{-1} peak to symmetric bending vibrations of Si-O-Si and Al-O-Al [33, 34].

Table 1: Elemental bulk composition of the fly ash sample, as determined by XRF (major elements)

Composition	Weight %
SiO_2	49.30
TiO_2	2.01
Al_2O_3	34.00
Fe_2O_3	5.78
MnO	0.05
MgO	0.99
CaO	5.06
Na_2O	<0.01
K_2O	0.87
SO_3	0.24
P_2O_5	0.59
Cr_2O_3	0.07
NiO	0.05
V_2O_5	0.04
ZrO_2	0.08
Loss on Ignition	0.52
Total	99.63

In order to obtain a picture of the spatial distribution of the various components identified in fly ash, 2D Raman mapping was undertaken. From the 2D array of approximately 10 000 Raman spectra recorded on the sample, five different spectra could be identified. These spectra are presented in Figure 8 and wavenumber assignments for each component given in Table 2. The image in Figure 8 reflects the distribution of the various materials within the analyzed sample area. The red spectrum (b) is that of α-quartz crystallites with the strongest peak at 462 cm^{-1}. In the purple spectrum (c), the quartz peak at 462 cm^{-1} is also visible, with a triplet appearing at 860, 955 and 1008 cm^{-1}. These peaks can be attributed to phosphates and sulphates, in accordance with data obtained from XPS measurements, or may belong to an intermediate phase of mullite. It has been shown that the mullite Raman spectrum can vary considerably depending on the temperature of formation and other materials such as TiO_2 present in the sample [37].

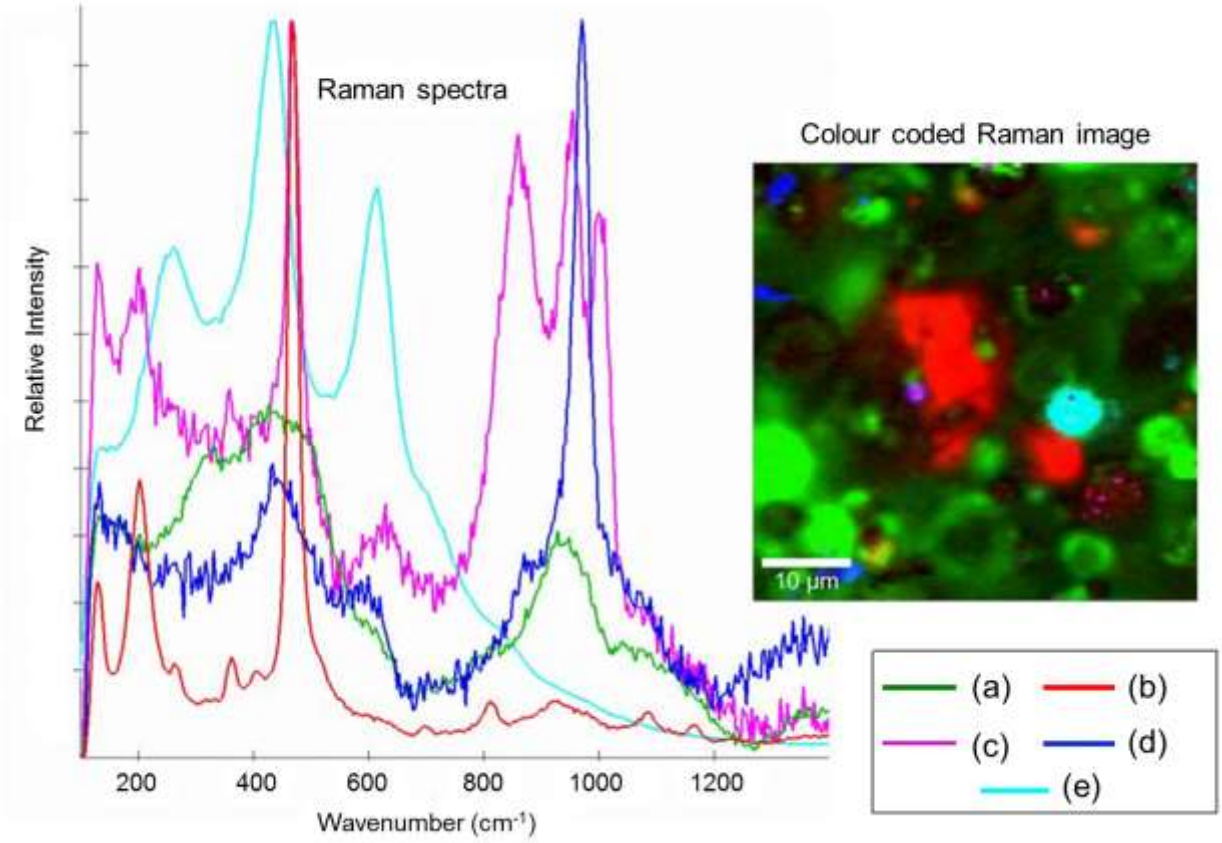

Figure 8: Raman spectra of the fly ash sample at different analysis points; (a) glass, (b) quartz, (c) quartz, phosphate and sulphate, (d) mullite and (e) rutile

The bands in the green spectrum (a) are broad and not very intense, which is typical for a glass. The Raman spectrum of mullite has its strongest peaks around 304, 408 and 965 cm^{-1} [37]. The 408 cm^{-1} peak overlaps with the first peak of an alumina/silicate glass representing Si-O bending vibrations at approximately 480 cm^{-1}, the spectrum is therefore a superimposition of various amorphous phases of mullite and silica glass.

In contrast, the very strong bands of rutile, the high temperature phase of TiO_2, can be observed in the aqua spectrum (e). The Raman cross-section of rutile is very large and therefore a strong Raman signal is obtained, even though rutile is only present in small quantities (see Table 2). The

blue spectrum (d), with a strong band at 965 cm^{-1} and smaller peaks at 304 and 408 cm^{-1} can be attributed to mullite. These results are summarised in Table 2.

Table 2: Main peaks in Raman spectra of components found in fly ash

Component	Wavenumber /cm^{-1} positions
α-quartz	462 *(vs)*, 358 *(sm)*, 206 *(m)*
Mullite	1104, 965 *(vs)*, 408, 304,
Rutile (high temperature phase TiO_2)	613 *(s)*, 430 *(vs)*, 258 *(s)*, 153 *(sm)*
Alumina silica glass	~480 *(br)*, ~1000 *(br)*
Calcium sulphate	1002 *(vs)*
Calcium phosphate	961 *(vs)*

vs :very strong, m: medium sm: small, br: broad

It is clear from the image that the main phase of the fly ash is amorphous silica glass and amorphous mullite (green). It also shows that crystalline quartz (red) is embedded in the spheres, but as separate crystallites. Rutile (aqua) is also not homogenously distributed, but interestingly enough the image is spherically shaped and probably formed a layer around one of the glass spheres. Crystalline mullite (blue) is also sparse. It has been observed that nano-mullite crystals are not easily observed with Raman spectroscopy and only larger particles can be detected.

In most of the Raman spectra the two typical broad peaks at ~1350 and ~1600 cm^{-1} representing amorphous carbon was observed (not shown) indicating that the carbon in this sample is amorphous, and not graphitic as previously observed by Chen [30] in a different fly ash sample.

3.2 Surface properties of the fly ash sample

3.2.1 Auger Electron Spectroscopy (AES)

Auger Electron Spectroscopy analysis of individual in-plume and in-stack fly ash particles has been reported by Hock and Lichtman [38]. The results obtained by these authors have shown significant

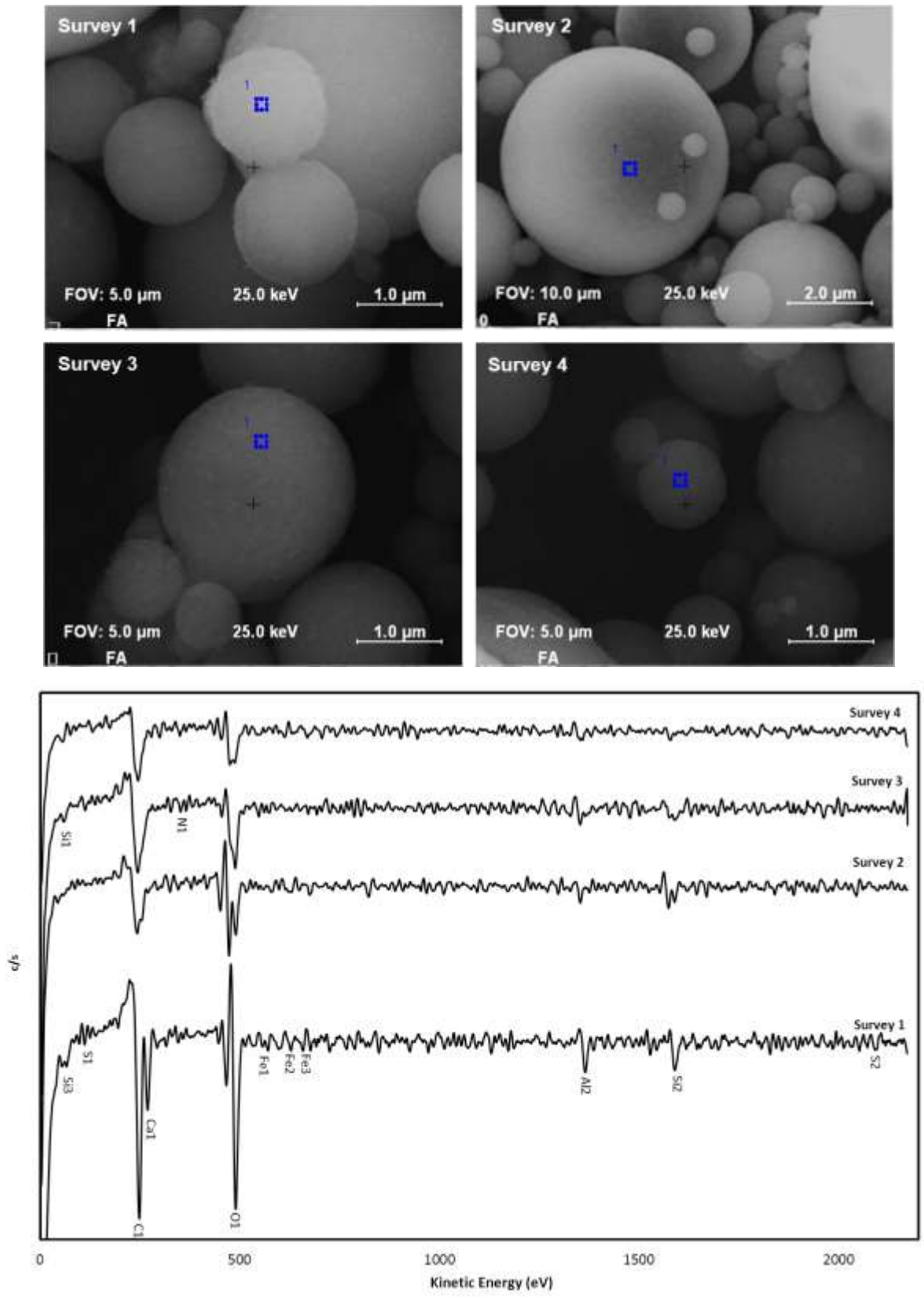

Figure 9: (a) SEM micrographs, areas chosen to perform the survey tests, and (b) corresponding spectra obtained from Auger electron spectroscopy analysis

inconsistency in the surface composition of individual fly ash particles within a particle range of 5 - 30 µm.

Using the SEM images obtained by the Scanning Auger Nanoprobe instrument, 12 fly ash particles, with varying particle sizes, were randomly chosen to perform the survey test in our study. The SEM micrographs, areas chosen to perform the survey tests and corresponding AES spectra of 4 of these fly ash particles are presented in Figure 9 while a summary of the elemental surface composition is presented in Figure 10. Carbon, oxygen, silicon, aluminium and calcium are the main constituents of the fly ash surface while small amounts of iron, sulphur and nitrogen were detected on some of the fly ash spheres. Figure 10 confirms a wide variation in elemental composition between particles. However, the main constituents were noticed on most of the spheres.

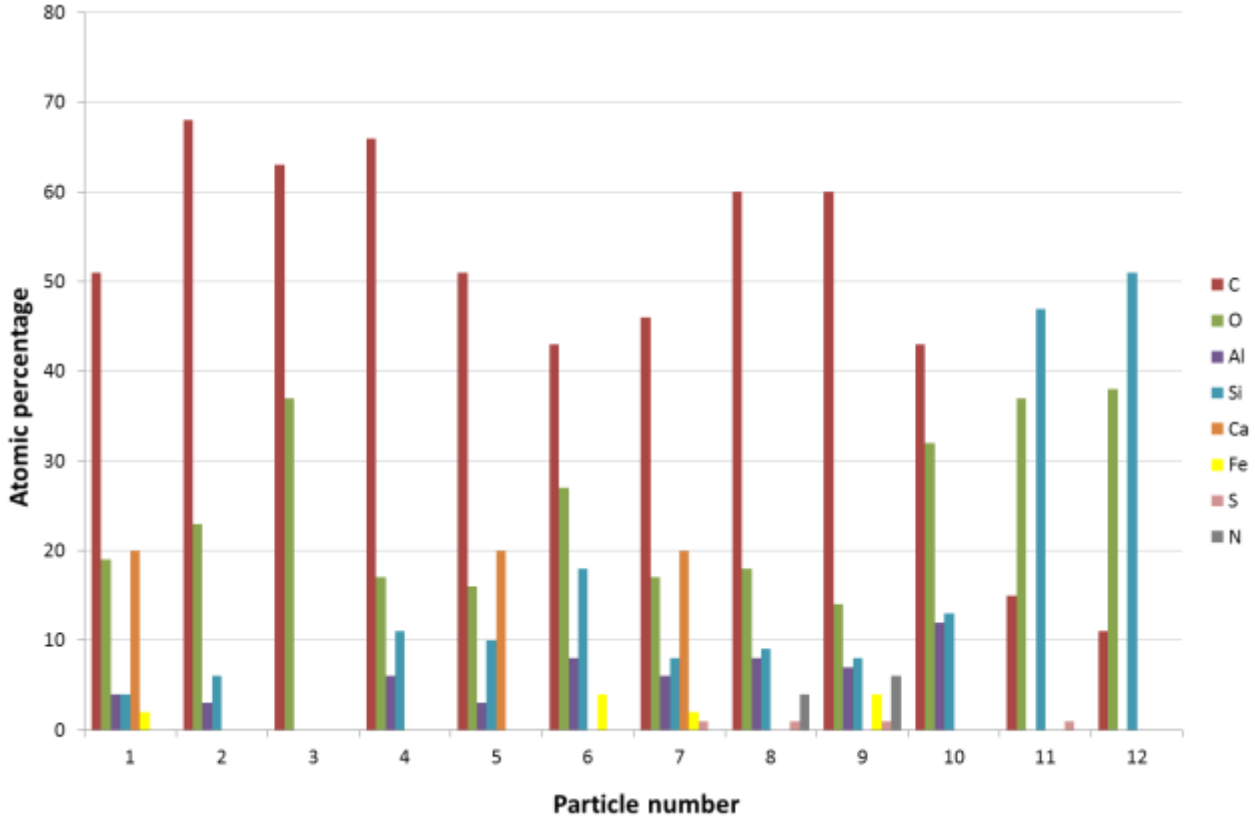

Figure 10: Auger Electron Spectroscopy Survey results, reported as atomic percentage per element, as obtained from measurements performed on 12 fly ash particles.

3.2.2 X-ray photoelectron spectroscopy (XPS)

XPS analysis is widely used for quantitative and qualitative analysis and to determine the chemical state of elements on the surface of solid materials. A typical XPS survey spectrum obtained from the analysis of the fly ash sample is presented in Figure 11. Confirming the results obtained from AES measurements, the main constituents of the near surface region are oxygen, carbon, silicon, aluminium and calcium. Iron and sulphur were detected in small quantities. Similar results were reported from XPS measurements of a fly ash sample by Mollah [39]. The XPS data was further analyzed by peak fitting, and the results obtained are summarized in Table 3.

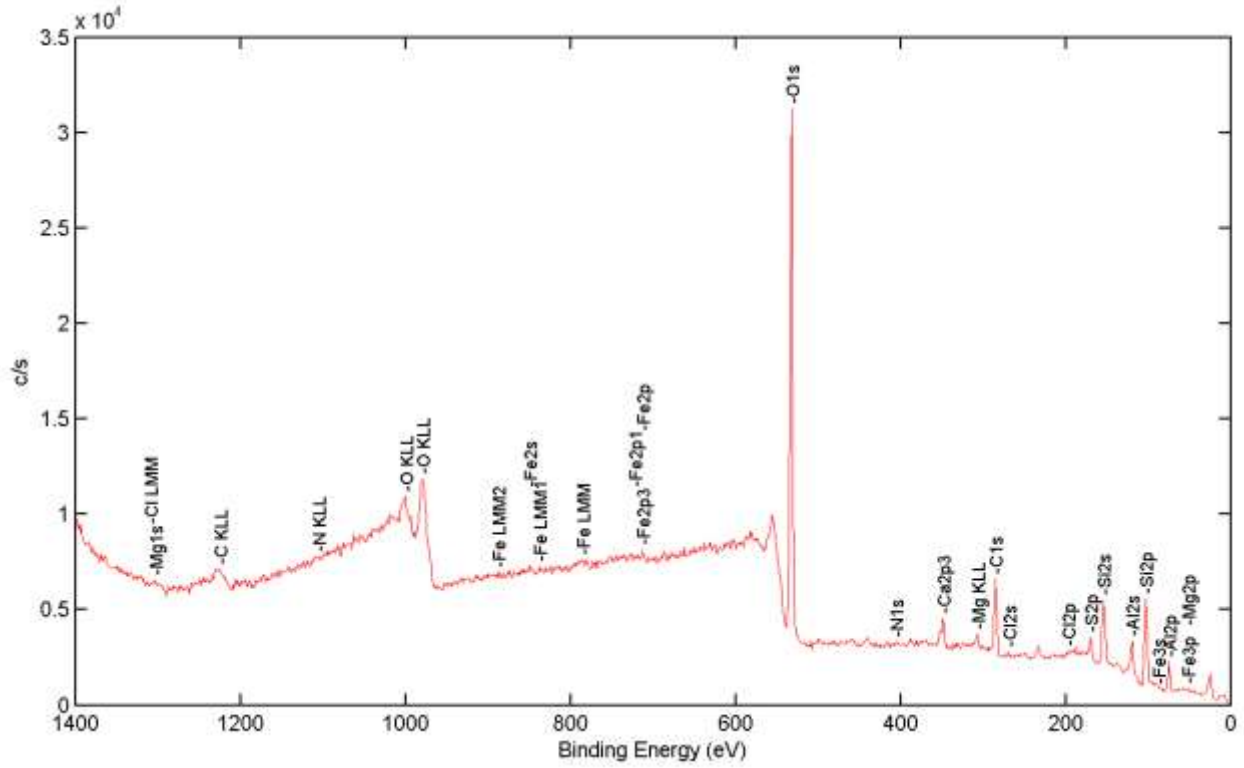

Figure 11: XPS survey spectrum of the fly ash sample

Table 3: Binding energies (obtained from peak deconvolution) and possible chemical states of the elements occurring at the surface of the fly ash sample, as obtained by XPS measurements

Element	Binding energy (eV)	Possible chemical states
O1s	531.3	$CaSO_4$
	532.5	SiO_2
Si2p	103	Silicate
Al2p	74.9	Halides/Oxide
Ca2p	348.3	$CaSO_4$
	349.4	$CaSO_x$; x<4
	351.9	$CaSO_4$
	353.0	$CaSO_x$; x<4
S2p	169.4	Sulphate
	170.6	Sulphate

3.3 Comparison of bulk and surface techniques

The data obtained from different quantitative analysis techniques have been summarized in Figure 12. The results obtained from AES and XPS measurements indicate that the surface composition of the fly ash spheres is considerably different from the composition of the bulk material, particularly in terms of the carbon content. The carbon contained in the fly ash sample seems to be concentrated on the surface of the spheres, confirming the observations made from SEM and TEM measurements.

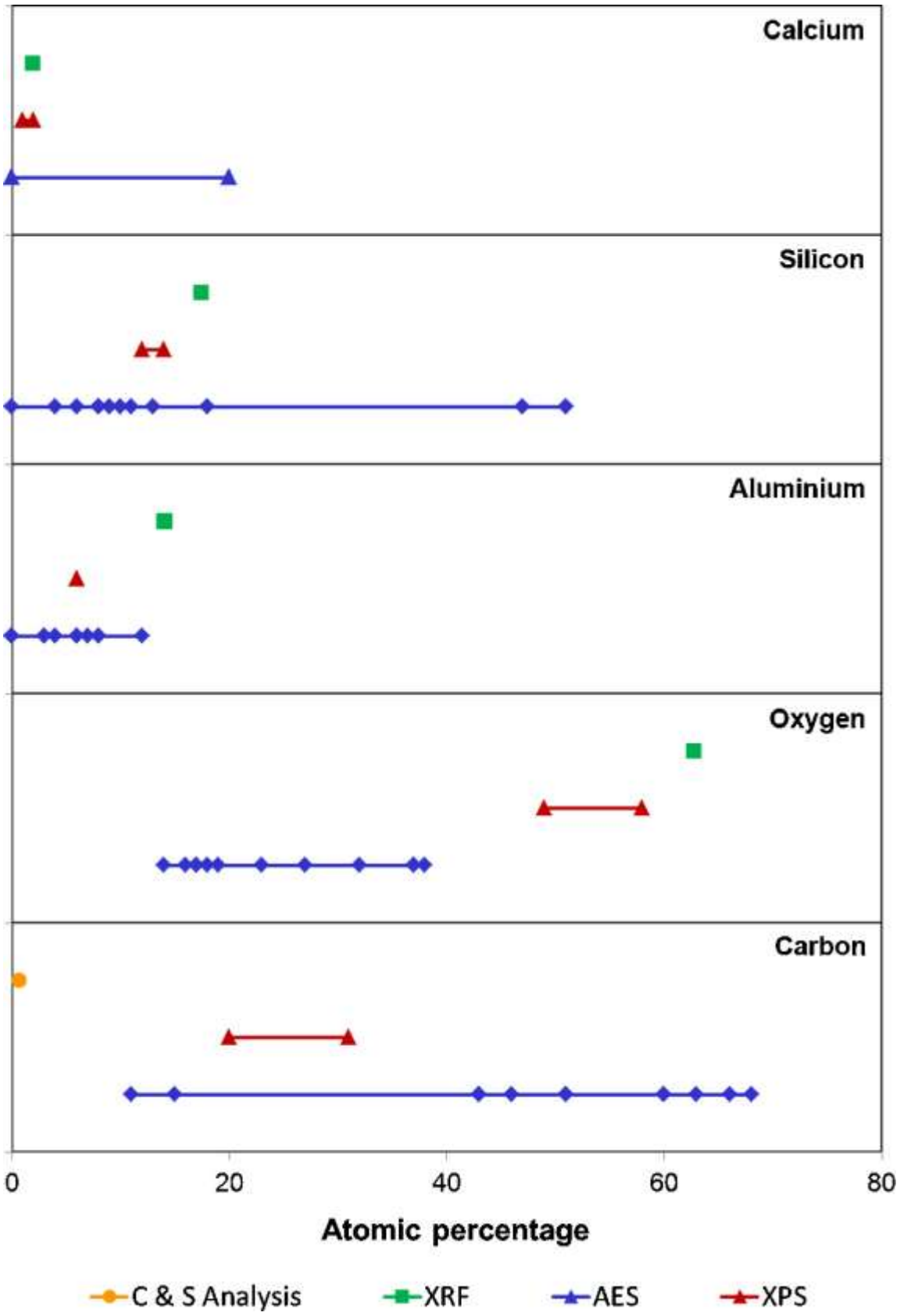

Figure 12: Comparison between the surface and bulk elemental composition of the ultrafine fly ash sample as determined by XRF, Carbon and Sulphur analysis, AES and XPS.

4. Conclusion

The surface, chemical and morphological properties of a South African coal fly ash sample classified as ultrafine were obtained by using a number of analytical techniques. XRD analysis has shown that 62% of the fly ash is in the amorphous glass phase, and that the main crystalline phases are mullite and quartz. The chemical composition as determined by XRF analysis has confirmed that this is a Class F fly ash, with low CaO content.

The spherical morphology and small particle size of the fly ash may enhance its applicability as filler in polymers. TEM analysis has indicated that this sample has a relatively smooth surface topography, with few agglomerates on its surface.

The phases detected in the Raman and FTIR spectra are in line with the XRD data, and the Raman image that was generated with the Raman spectra gives a good spatial representation of the distribution of the different phases in the sample.

The sample showed a very low weight loss for temperatures ranging between 25 and 1000°C. This can be an added advantage when using fly ash as filler in polymers because the filler will be thermally stable with low volatility at general polymer processing temperatures.

AES and XPS results have confirmed a wide variation in surface composition between fly ash spheres, indicating that surface modification techniques of this sample may prove to be challenging. The composition of the fly ash surface is significantly different from the bulk sample, and therefore surface characterisation is important when considering compatibility between matrices when applying this sample as filler in polymers.

Acknowledgements

The authors acknowledge the NRF, the Ernst Oppenheimer Memorial Trust and Ash Resources (Pty Ltd) for financial assistance. The latter also provided the studied fly ash sample. Dr Richard

Kruger is acknowledged for his valuable intellectual contribution, Ms Wiebke Grote for XRD, Ms Jeanette Dykstra for XRF, and the University of Pretoria Laboratory for Microscopy and Microanalysis for assistance with AFM, SEM and TEM. EMvdM thanks the University of Pretoria for granting her sabbatical leave to complete this study.

This work is based on the research supported in part by the National Research Foundation of South Africa (Grant number TP1207314969). The Grantholder acknowledges that opinions, findings and conclusions or recommendations expressed in any publication generated by the NRF supported research are that of the author(s), and that the NRF accepts no liability whatsoever in this regard.

References

[1] R.A. Kruger, Fly ash beneficiation in South Africa: creating new opportunities in the market-place, Fuel 76(8) (1997) 777-779.

[2] Eskom. Ash management in Eskom. Factsheet CO 0004 Revision 9 (January 2013), www.eskom.co.za/c/25/facts-figures/

[3] J.S. Mahlaba, E.P. Kearsley, R.A. Kruger, Physical, chemical and mineralogical characterisation of hydraulically disposed fine coal ash from SASOL Synfuels, Fuel 90 (2011) 2491–2500.

[4] E.P. Kearsley, P.J. Wainwright, The effect of fly ash properties on concrete strength, J. S. Afr. Inst. Civ. Eng. 45(1) (2003) 19-24.

[5] C.D. Woolard, K. Petrus, M. van der Horst. The use of a modified fly ash as an adsorbent for lead, Water SA 26(4) (2000) 531-536.

[6] W.M. Gitari, L.F. Petrik, O. Etchebers, D.L. Key, C. Okujeni, Utilization of fly ash for treatment of coal mines wastewater: Solubility controls on major inorganic contaminants, Fuel 87 (2008) 2450–2462.

[7] V. Somerset, L. Petrik, E. Iwuoha, Alkaline hydrothermal conversion of fly ash precipitates into zeolites 3: The removal of mercury and lead ions from wastewater, J. Environ. Manage. 87 (2008) 125–131.

[8] R.H. Matjie, J.H. Bunt, J.H.P. van Heerden, Extraction of alumina from coal fly ash generated from a selected low rank bituminous South African coal, Miner. Eng. 18 (2005) 299–310.

[9] A. Shemi, R.N. Mpana, S. Ndlovu, L.D. van Dyk, V. Sibanda, L. Seepe, Alternative techniques for extracting alumina from coal fly ash, Miner. Eng. 34 (2012) 30–37.

[10] J.C. Swanepoel, C.A. Strydom, Utilisation of fly ash in a geopolymeric material, Appl Geochem. 17 (2002) 1143–1148.

[11] S.M. Nyale, O.O. Babajide, G.D. Birch, N. Böke, L.F. Petrik, Synthesis and characterization of coal fly ash-based foamed geopolymer, Procedia Environ. Sci. 18 (2013) 722 – 730.

[12] G.M. Muriithi, L.F. Petrik, W.M. Gitari, F.J. Doucet, Synthesis, characterisation and potential CO_2 capture properties of a novel adsorbent (hydrotalcite) from South African coal-combustion fly ash, Abstract of the 12th International Chemical Conference Africa, Pretoria, South Africa, (2013), 8-12 July.

[13] K. Reynolds, R. Kruger, N. Rethman, W. Truter, The production of an artificial soil from sewage sludge and fly-ash and the subsequent evaluation of growth enhancement, heavy metal translocation and leaching potential, ISBN 1-86845-946-2, Water SA Special Edition: WISA Proceedings 2002. Available from http://www.wrc.org.za

[14] G.N. Muriithi, L.F. Petrik, O. Fatoba, W.M. Gitari, F.J. Doucet, J. Nel, S.M. Nyale, P.E. Chuks, Comparison of CO_2 capture by ex-situ accelerated carbonation and in in-situ naturally weathered coal fly ash, J. Environ. Manage. 127 (2013) 212-220.

[15] R.A. Kruger, M. Hovy, D. Wardle, The use of fly ash fillers in rubber, 1999 International Ash Utilization symposium, Center for Applied Energy Research, University of Kentucky, Lexington, KY, Paper #72. Available from www.flyash.info

[16] S.V. Vassilev, R. Menendez, D. Alvarez, M. Diaz-Somoano, M.R. Martinez-Tarazona, Phase-mineral and chemical composition of coal fly ashes as a basis for their multicomponent utilization. 1. Characterization of feed coals and fly ashes, Fuel 82 (2003) 1793 - 1811.

[17] S.S. Potgieter-Vermaak, J.H. Potgieter, R.A. Kruger, Z. Spolnik, R.A. van Grieken, Characterisation of the surface properties of an ultra fine fly ash (UFFA) used in the polymer industry, Fuel 84 (2005) 2295-2300.

[18] O.S. Ayanda, O.S. Fatoki, F.A. Adekola, B.J. Ximba, Characterization of Fly Ash Generated from Matla Power Station in Mpumalanga, South African E-Journal of Chemistry 9(4) (2012) 1788-1795.

[19] A.C. Roulin-Moloney, W.J. Cantwell, H.H. Kausch, Parameters determining the strength and toughness of particulate-filled epoxy resins, Polym. Compos. 8(5) (1987) 314–23.

[20] Y.Y. Nakamura, M. Yamaguchi, M. Okubo, T. Matsumoto, Effects of particle size on mechanical and impact properties of epoxy resin filled with spherical silica, J. Appl. Polym. Sci. 45(7) (1992) 1281–9.

[21] ASTM C 618-93, Standard Specification for Fly Ash and Raw or Claimed Natural Pozzolan for Use as Mineral Admixture in Portland cement Concrete, Annual Book of ASTM Standards, vol. 04.02, pp. 310-312.

[22] EN 206-1, European Committee for Standardization. NBN EN 206-1. Concrete - Part 1: specification, performance, production and conformity, 2000.

[23] O. Senneca, Burning and physico-chemical characteristics of carbon in ash from a coal fired power plant, Fuel 87 (2008) 1207–1216.

[24] N.J. Wagner, R.H. Matjie, J.H. Slaghuis, J.H.P. van Heerden, Characterization of unburned carbon present in coarse gasification ash, Fuel 87 (2008) 683–691.

[25] M.A. Gabal, D. Hoff, G. Kasper, Influence of the atmosphere on the thermal decomposition kinetics of the $CaCO_3$ content of PFBC coal flying ash, J. Therm. Anal. Calorim. 89(1) (2007) 109–116.

[26] B. Rubio, M.T. Izquierdo, M.C. Mayoral, M.T. Bona, R.M. Martínez-Tarazona, Preparation and characterization of carbon-enriched coal fly ash, J. Environ. Manage. 88 (2008) 1562–1570.

[27] J. Payá, J. Monzó, M.V. BorracheroV, E. Perris, F. Amahjour, Thermogravimetric Methods for Determining Carbon Content in Fly Ashes, Cem. Concr. Res. 28(5) (1998) 675-686.

[28] J.M. Bigham, D.A. Kost, R.C. Stehouwer, J.H. Beeghly, R. Fowler, S.J. Traina, W.E. Wolfe, W.A. Dick, Mineralogical and engineering characteristics of dry flue gas desulfurization products, Fuel 84 (2005) 1839–1848.

[29] T. Shimizu, K. Matsuoka, T. Niki, Decomposition of $CaSO_4$ in the presence of coal ash, Nippon Enerugi Gakkai Sekitan Kagaku Kaigi Happyo Ronbunshu 42 (2005) 51-52. In Japanese.

[30] Y. Chen, N. Shah, F.E. Huggins, G.P. Huffman, Transmission Electron Microscopy Investigation of Ultrafine Coal Fly Ash Particle, Environ. Sci. Tech. 39 (2005) 1177–1151.

[31] J.C. Hower, A. Dozier, M.T. Tseng, R.A. Khatri, Association of the Sites of Heavy Metals with Nanoscale Carbon in a Kentucky Electrostatic Precipitator Fly Ash, Environ. Sci. Tech. 42 (2008) 8471–8477.

[32] C.M. Demanet, Atomic force microscopy determination of the topography of fly ash particles, Appl. Surf. Sci. 89 (1995) 97-101.

[33] D. Voll, P. Angerer, A. Beran, H. Schneider, A new assignment of IR vibrational modes in mullite, Vib. Spectrosc. 30 (2002) 237-243.

[34] A. Fernańdez-Jimeńez, A. Palomo, Mid-infrared spectroscopic studies of alkali-activated fly ash structure, Micropor. Mesopor. Mat. 86 (2005) 207–214.

[35] R.K. Vempati, A. Rao, T.R. Hess, D.L. Cocke, H.V. Lauer Jr, Fractionation and Characterization of Texas Lignite Class 'F' Fly Ash by XRD, TGA, FTIR and SFM, Cem. Concr. Res. 24(6) (1994) 1153-1164.

[36] P. Chindaprasirt, C. Jaturapitakkul, W. Chalee, U. Rattanasak, Comparative study on the characteristics of fly ash and bottom ash geopolymers, Waste Manage. 29 (2009) 539–543.

[37] S. Shoval, M. Boudeulle, S. Yariv, I. Lapides, G. Panczer, Micro-Raman and FT-IR spectroscopy study of the thermal transformations of St. Claire dickite, Opt. Mater. 16 (2001) 319-327.

[38] J.L. Hock, D.A. Lichtman, A comparative study of in-plume and in-stack collected individual coal fly ash particles, Atmos. Environ. 17(4) (1983) 849-852.

[39] M.Y.A. Mollah, T.R. Hess, D.L. Cocke, Surface and Bulk studies of leached and unleached fly ash using XPS, SEM, EDS and FTIR techniques, Cem. Concr. Res. 24 (1994) 109-118.